Amplified plasmonic and microfluidic setup for DNA monitoring

J. Rafaela Guerreiro[1*], Andrey Ipatov[1], Joana Carvalho[1], Anna Toldrà[2], Marta Prado[1]

[1]INL – International Iberian Nanotechnology Laboratory, Department of Life Sciences, 4715-330, Braga, Portugal

[2]IRTA, 43540, Sant Carles de la Ràpita, Tarragona, Spain

Address correspondence to:

joanarlguerreiro@gmail.com

ORCID - 0000-0001-8719-1978

Current Address:

Polytech Inst Porto ISEP, BioMark CEB UM,

Rua Dr Antonio Bernardino de Almeida 431, P-4249015

Porto, Portugal

Keywords: Signal amplification, microfluidic cell, Localized Surface Plasmon Resonance, oligonucleotides detection, Label-free amplification, plasmonic sensors.

Abstract

Plasmonic nanosensors for label-free detection of DNA require excellent sensing resolution, which is crucial when monitoring short DNA sequences, as these induce tiny peak shifts, compared to large biomolecules. We report a versatile and simple strategy for plasmonic sensors signal enhancement by assembling multiple (four) plasmonic sensors in series. This approach provided a four-fold signal enhancement, increased signal to noise ratio, and improved sensitivity for DNA detection. The response

of multiple sensors based on AuNSpheres was also compared to AuNRods with the latter showing better sensing resolution.

The amplification system based on AuNR was integrated with a microfluidic platform and applied to the monitoring of DNA, specific from environmental invasive species - zebra mussels. DNA from zebra mussels was log concentration-dependent from 1 pM to 1×10^6 pM, reaching a detection limit of 2.0 pM. In situ tests were also successfully applied to real samples, within less than 45min, using DNA extracted from zebra mussel meat.

The plasmonic nanosensors' signal will be used as a binary output (YES/NO) to assess the presence of those invasive species. Even though these genosensors were applied to the monitoring of DNA in environmental samples, they also offer a great advantage in a wide range of fields, such as disease diagnostics.

Introduction

Gold nanostructures are known for their bright colors, presenting unique optical features[1]. When interacting with light the electrons at the surface of the nanostructure start to collectively oscillate exhibiting a phenomenon called localized surface plasmon resonance (LSPR), within the visible to near-infrared frequencies. This collective oscillation leads to strong light scattering which results in resonance peaks in their extinction spectra. The plasmon peak position and intensity of gold nanostructures strongly depend on its composition, geometry, size, interparticle spacing, surface density, and refractive index of the surrounding medium[2, 3]. Nanoplasmonic biosensors are fabricated targeting the formation of nanostructures on a surface through top-down conventional lithography techniques (electron beam lithography, ion beam lithography, colloidal lithography)[4–6] or bottom-up approaches, based on the deposition of pre-synthesized nanostructures onto the surface[7, 8]. Bottom-up methodologies offer the simplest, cheapest, and fastest fabrication alternatives, without requiring specialized equipment and setup. Moreover, nanoparticles (NPs) synthesis has the advantage to produce inexpensively large amounts of single crystal particles with the freedom to select the type of materials, shapes, sizes, and to tune their LSPR frequency[9–11].

The optical properties of plasmonic sensors rely on the intrinsic properties of the assembled NP, in their spatial arrangement and surface interactions. Therefore, it is crucial to select immobilization strategies and working conditions to achieve the highest NP density with optimum inter-particle spacing arrangement to minimize plasmon coupling effects and achieve narrow and intense plasmon peaks, as these highly contribute to the sensing performance of plasmonic biosensors.

Plasmonic sensors, due to its highly confined electromagnetic field, are extremely sensitive to changes in the dielectric environment close to the surface. The presence of a target molecule alters the refractive index around the nanostructures, inducing maximum extinction peak shifts to higher wavelengths. Sensing resolution depends on the absolute magnitude and narrow bandwidth of the plasmon peak, to accurately track the shifts of maximum extinction peak[2]. Thus, the spatial arrangement of the nanostructures and the sensing resolution are directly related. Sensing resolution is particularly relevant when monitoring small molecules which, induce tiny peak shifts compared to large biomolecules, such as proteins or enzymes[12]. Therefore, the narrower the bandwidth, the sharper the plasmon peak gets, and consequently the easier it will be to track tiny peak shifts. However, assembling a well-dispersed monolayer of single NPs distribution with high surface density and reduced plasmon coupling is a compromise difficult to achieve for bottom-up approaches, even when controlling crucial factors such as time, particle concentration in solution and temperature[13, 14]. Aggregates and clusters formation on the surface of plasmonic sensors triggers LSPR peak broadening due to interparticle coupling and, consequently, decrease the overall NPs surface area and sensitivity.

Here, we present an alternative strategy for signal amplification of plasmonic sensors based on multiple plasmonic sensors in series to maximize NPs surface density and achieve high sensitivity and reproducibility performance, overcoming signal intensity limitations of bottom-up approaches. This strategy is based on a flow cell that assembles multiple plasmonic sensors, integrated in a microfluidic system to detect DNA from invasive species within less than 45 min, without labels, enzymes, or complex DNA structures amplifications steps. Integration of the microfluidic systems allows the continuous monitoring of plasmon peak shifts of the same region, as sensors remain exactly in the same

position, mitigating manipulation errors. The developed setup can be applied to all plasmonic sensors regardless of the fabrication strategy.

Additionally, the device was used to monitor invasive species, zebra mussel (*Dreissena Polymorpha*) in river basins samples from Spain. Zebra Mussels are one of the 100 most harmful invasive alien species in the world and a global threat to biodiversity and economy[15]. These species can rapidly spread, being difficult to predict possible contaminated regions. Additionally, eliminating contaminated regions is usually temporary and costly. Therefore, its early detection through environmental DNA would allow their identification and implementation of timely measures to mitigate their negative impact[16].

Experimental Section

Fabrication of LSPR nanosenors based on Gold Nanospheres (AuNS) and Gold NanoRods (AuNR)

Synthesized 80 nm AuNS were immobilized onto the glass surface by physical adsorption. To prepare plasmonic sensors, the glass surfaces modified with a positively charged polymer were immersed overnight in the NP solution. Regarding AuNR plasmonics sensors, the substrates were chemically modified with a mercapto silane compound prior its immersion on AuNR solution overnight. Detailed fabrication procedures and characterization of both NPs and plasmonic sensors are described in the experimental section of SI.

Fabrication of Signal Amplification home-made flow cell

Signal amplification flow cell was built by combining the plasmonic sensors, the polydimethylsiloxane (PDMS) soft layers, and the polymethylmethacrylate (PMMA) transparent solid supports, as shown in **Fig. 1A**. Each PDMS layer is the result of two PDMS semi-layers (0.25 mm thickness) with engraved half channels (obtained by direct PDMS reagent cast onto the PMMA micromold, shown in **Fig. 1B**) which, bonded together, forming the 3D channels inside the PDMS layer. The two PDMS layers prepared exhibit distinct channel designs and similar openings for a good optical path alignment with each other, **Fig. 1C (PDMS layers 6/7)**.

The flow-cell is assembled by intercalating the three PMMA supports, four nanoplasmonic sensors/glass substrates and two PDMS thin layers. Briefly, the horizontally assemble is made by: i) placing a PMMA support on the bottom (5), ii) glass /plasmonic sensor, iii) PDMS layer (6), iv) glass /plasmonic sensor, v) the PMMA spacer (3), vi) glass/plasmonic sensor, vii) the PDMS layer (7), viii) glass/plasmonic sensor and ix) finally the top PMMA support (1), hold together with a PMMA square "ring" (**Fig. 1D/E**).

To create the flow chamber in each PDMS layer, two plasmonic sensors/glass substrate are required, blocking the fluid from lateral escaping, and forcing the flow to move in the up direction. The fluid enters the flow cell through one connector at the top of the PDMS layers (6) and gets inside the optical chamber through the bottom, minimizing formation of air bubbles. Then, it flows to the second PDMS through the middle connection of the PMMA, enter the chamber through the bottom, passes again through the middle connection of PMMA, enters the first PDMS and leaves the flow cell, as shown in scheme of **Fig. 1F**. A photograph and additional fabrication details of the microfluidic flow cell are described in the SI (**Fig. S1**).

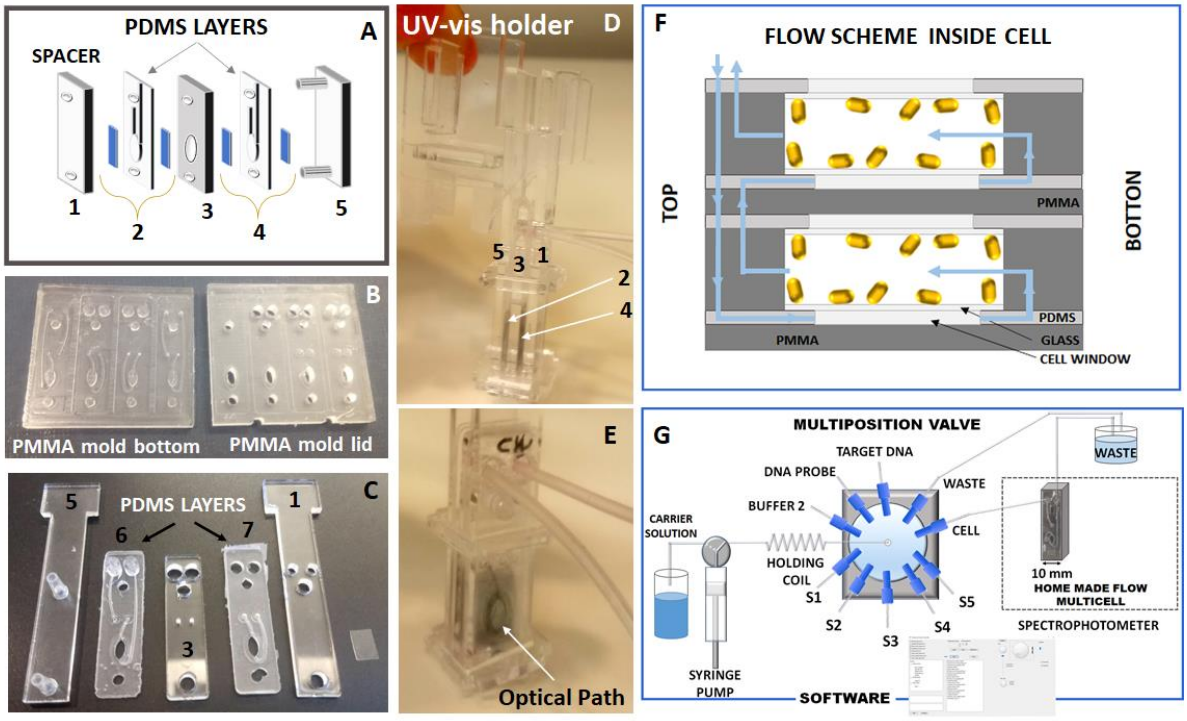

Fig. 1. Overview of the microfluidic cell and system. **A)** Scheme of flow cell assembly with plasmonic sensors or plain glass (**2 and 4)** to be placed before and after the PDMS layers; **B)** PMMA mold for PDMS thin layers production; **C)** Flow cell components: bottom PMMA spacer **(5)**, bottom PDMS layer **(6)**, middle PMMA spacer **(3)**, top PDMS layer **(7)** and top PMMA layers **(1)**, left to right; **D)** Image of the assembled flow cell, lateral view (standard cuvette size 10×10×45 mm); **E)** Image of assembled flow cell, front view; **F)** Flow direction inside the microfluidic cell; **G)** Automated flow injection system used in the detection, S1-S5: sample/standard solution dilutions.

Microfluidic LSPR sensor measurements

The versatility of the developed flow cell allows to conduct the measurements with single or multiple plasmonic sensors (up to four). The flow cell was connected to an automated flow injection system controlled by a homemade software, that also controlled the UV-vis, as displayed in **Fig. 1G** (**Fig. S2/S3** of SI).

Recipe protocols used in all experiments are detailed in **Table S1** and **S2** of SI. All LSPR spectra, for standards and samples, were collected for wavelength ranging from 400 to 800 nm. To determine the extinction maximum wavelength - λ_{max} (peak wavelengths), MATLAB R2018 software was used to interpolate each spectrum by fitting a polynomial function of degree 2, from 480–580 nm and 570-670 nm for AuNS and AuNR, respectively. This strategy allows to monitor the peak position below the wavelength resolution of the spectrophotometer.

Real-time immobilization of probe DNA followed by target hybridization

Nanoplasmonic sensors based on AuNR were used to monitor different strategies for DNA probe immobilization followed by target DNA detection (hybridization). All the synthetic oligonucleotides sequences included a 5' Thiol C6 end modification with and without a polyA oligonucleotides-spacer. DNA probes fully complementary to the target DNA are specific sequences from zebra mussel (*Dreissena Polymorpha*), one of the 100 most harmful invasive alien species in the world[17]. Co-immobilization of DNA probe with Poly (ethylene glycol) methyl ether thiol- mPEG of different

molecular weights (Mw), 350, 800 and 2000 Da, at different concentrations was also evaluated. The oligonucleotides sequences used are shown in **Table 1**.

Table 1. Oligonucleotides sequences used as capture probe and target.

	Sequence (5' to 3')	Bases
HS-C6-polyA-ssDNA Probe (SH-polyA-DNA)	Thiol C6 – AAAAAAAAAATATTCGTTTAGAGCTAAGGGC	10 + 21
HS-C6 -ssDNA Probe (SH-DNA)	Thiol C6 –TATTCGTTTAGAGCTAAGGGC	21
Full Match Target DNA	GCCCTTAGCTCTAAACGAATA	21

Probe DNA immobilization was performed in running buffer 0.99M $CaCl_2$.TE buffer pH 7.4 (buffer 1) while hybridization studies were conducted in 0.99 M $CaCl_2$.TE buffer pH 8.4 (buffer 2). This way the prepared running buffers match the buffer concentration in the standards/samples eliminating RI changes inherent to the buffer.

Probe immobilization and hybridization experiments were conducted with the flow cell assembled with 4 nanoplasmonic sensors based on AuNR, at room temperature (22ºC). The study of different surface modifications was performed by incubating probe and/or PEG for ~1h, followed by 3×10^6 pM of target DNA for ~4h at intermittent flow (according to **Table S2 of SI** in the hybridization studies column).

Calibrations with increasing target concentrations ranging from 1pM to 1×10^6 pM were incubated for ~45 min each (according to **Table S2 of SI** in the calibration column). The real samples analysis used 20 μL of Zebra Mussel extract diluted in 280 μL of hybridization buffer (buffer2) for a 15-fold dilution. Similarly, to the standard solution, the Zebra Mussel samples were incubated for 45 min at intermittent flow. All the details on sample preparation and analysis protocol are further explained in SI or displayed in **Table S2**. Experimental details on DNA surface coverage assay during co-immobilization with mPEG are also explained in experimental section of SI.

All spectra were collected in the suitable buffer before and after each surface modification, under continuous flow of 1μL s^{-1}.

RESULTS AND DISCUSSION

Fabrication of plasmonic sensors

Prior plasmonic sensors fabrication, the NPs were synthesized via a wet chemical method for fast production of large amounts of uniform NPs. AuNS and AuNR were characterized by UV-vis adsorption, with spectra showing the maximum LSPR peak at 551.9 nm and 528.3 nm/662.1 nm for the transverse/longitudinal peak, respectively. Size estimation was obtained by TEM image analysis, showing a size of 78.9 ± 7.4 nm for AuNS, whereas AuNR showed width × length dimensions of 17.7 ± 2.2 × 42.3 ± 4.2 nm (aspect ratio of 2.3), as shown in **Fig. S4** of SI. Before the NP attachment onto the glass substrate, excess of capping agents was removed to facilitate the covalent immobilization. This step is especially important for AuNR, as CTAB surfactant adversely affect the surface assembly, due to the predominant electrostatic shielding effect to stabilize the colloids and consequently the diffusion of AuNR to the surface becomes secondary [18]. Although for AuNS, the effect of citrate capping agent is not problematic, as the self-assembly of nanoparticles into the surface, is driven by electrostatic interactions, which are strengthened by the negative surface charge of citrate/AuNS. Electrostatic interactions and silane coupling chemistry were the two strategies used to attach AuNS and AuNR, respectively. In the case of AuNS, to minimize repulsion between the negatively charged glass surfaces (activated hydroxylate groups) and NPs, a positively charged PDDA polymer was added to the glass surface. The electrostatic repulsion within the like-charged AuNS results in a minimum distance between neighboring AuNS on the substrate, forming a short-range ordered pattern. For the preparation of AuNR base sensors, chemical immobilization was obtained through a hetero-functional silane-thiol linker. The silane functional groups react with the hydroxyl groups on activated glass surface, while the exposed mercapto functional groups interact with AuNR, incubated at low CTAB concentrations. The mercapto functional groups of the linker stablish strong S-Au bonds with surface of AuNR, enabling its assembly. During the fabrication of plasmonic sensors, long incubation times of NPs might lead to the formation of multiple layers stacking however, to minimize this effect, low particles and stabilizing agents concentrations, were used (**Fig. S5** of SI). The presence of AuNS and

AuNR on the glass substrates was easily identified by the appearance of a light pink or blue color, respectively, as shown in **Fig. 2A.**

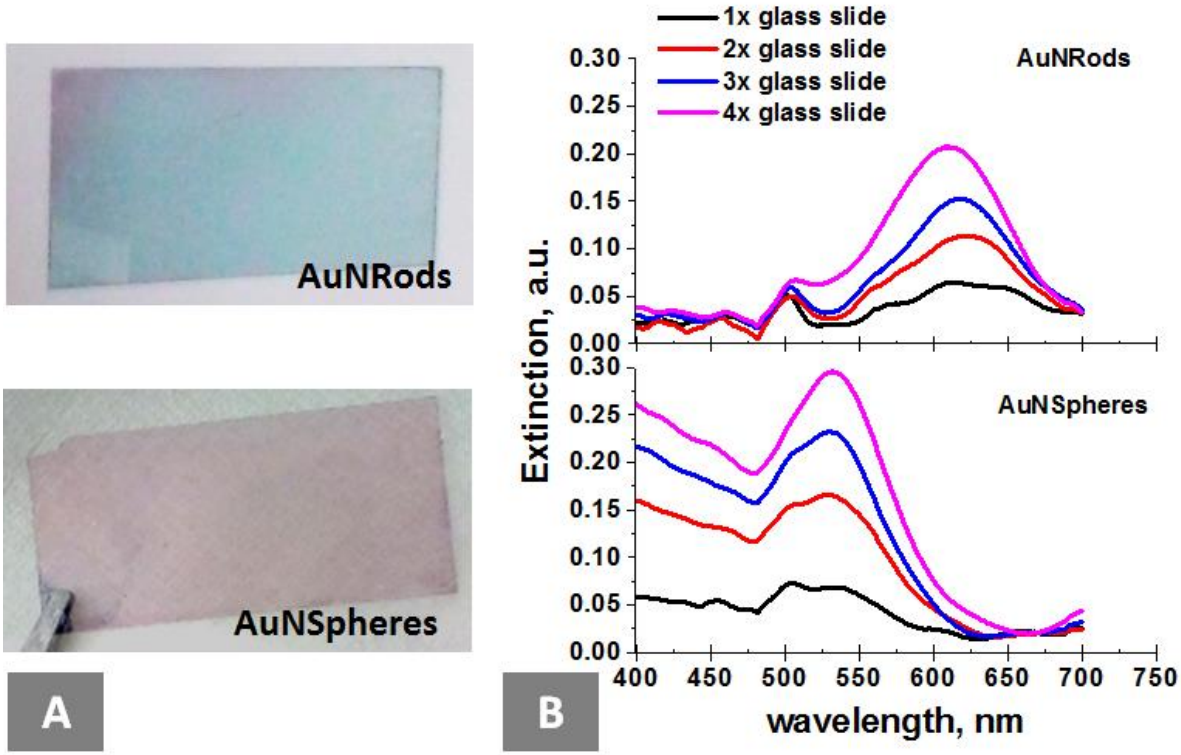

Fig. 2. A) Image of plasmonic sensors assembled with AuNR and AuNS, B) Effect of multiple plasmonic sensors for both AuNR and AuNS in air.

Characterization of nanoplasmonic sensors

The fabricated plasmonic sensors were characterized by UV-vis spectroscopy and showed extinction spectra with LSPR peaks at 532.8 nm for AuNS, while AuNR coated substrates displayed the longitudinal LSPR band at 614.7 nm and transverse LSPR band at 505.2 nm. The AuNS symmetric shape presented a single LSPR band while the anisotropy shapes, AuNR, showed two LSPR bands with different intensities[19]. The higher intensity of the longitudinal band is due to strong surface plasmon oscillations along the nanorod long axis when compared to the surface plasmon oscillations of the transverse LSPR band (plasmon oscillation along the nanorod short axis). As expected, the peak position of both NPs, in solution and at the surface, presented slightly distinct peak positions, due to the effect of the substrate on the LSPR spectra [20].

Bottom-up fabrication of plasmonic sensors influence dispersity, arrangement, and density of AuNP on the surface which determines intensity of optical responses, signal/noise ratio, and shape of the plasmon peaks (narrow/broad). The increase of plasmon coupling effect induces plasmon peak broadening and signal decrease due to its high NP distance-dependent. This distance has been calculated using plasmon hybridization models, demonstrating that distances of 2 to 2.5 times the particle diameter start to induce plasmon coupling[21]. The low NP density, low signal/noisy ratio, and the broadening of the LSPR bands challenge accurate small peak shifts monitoring.

Plasmonic sensors with both AuNS and AuNR displayed extinction spectra with lower band intensities (AuNR longitudinal band 0.06 a.u. and AuNS 0.07 a.u) when compared to its colloids, given the lower nanostructures density on the surface. However, the increase of NP density could directly lead to plasmon coupling effects.

Surface distribution and density were evaluated through SEM image analysis. Surface densities for AuNR and AuNS showed values of 131 particles μm^{-2} and 35 particles μm^{-2}, corresponding to a surface coverage of 7.5% and 17.6%, respectively (**Fig. S6**, SI). Based on the minimum inter-particle distance required to avoid coupling effect, the maximum NPs density was roughly estimated, with values of 281 particles μm^{-2} and 32 particles μm^{-2} for AuNR and AuNS, respectively. These data suggest that plasmon coupling is insignificant for AuNR while for AuNS it is close to the limit. The arrangement of AuNR on the glass substrate was also evaluated by Atomic Force Microscopy (AFM) indicating that most of the nanoparticles are horizontally displayed (**Fig. S7** of SI).

Amplification of plasmonic sensors signal

Signal enhancement, an increase of signal/noise ratio and increment of the global surface density without plasmon coupling effects were achieved through the reading of multiple plasmonic sensors. Additionally, the integration of the flow cell in a microfluidic system allows the continuous measurement of LSPR plasmon peaks shifts induced from surface changes of a specific region/area of the sensor, minimizing shifts variation and errors associated to sample replacement after each modification step.

Flow cell signal amplification capacity was evaluated by comparison of the extinction spectra in air of single and multiple plasmonic sensors. Collected spectra are displayed in **Fig. 2B**. Overall, the results showed an increase of signal intensity proportional to the increment of the number plasmonic sensors, for both AuNS and AuNR. The peak width of the spectra collected narrowed from single to 4 plasmonic sensors, for both shapes, assessed through the full width at half-maximum (FWHM) which decreased from 149 to 123 for AuNR and from 155 to 122 for AuNS. Additionally, collected data with single plasmonic sensors showed noisy spectra, being difficult to accurately estimate the maximum intensity and peak positions of the LSPR band. Nevertheless, a rough estimation through Lorentzian fitting was done. Single AuNR nanoplasmonic sensors showed the longitudinal LSPR peak position at 614.7 nm (0.0640 a.u.) whereas for AuNS based sensors the peak was at 532.8 nm (0.0680 a.u.). When four nanoplasmonic sensors were used, AuNR showed a longitudinal LSPR peak at 610.4 nm (0.2072 a.u.) and AuNS at 532.1 nm (0.2956 a.u.). In summary, the multiple plasmonic sensors in series lead to a 4-fold increase of the optical signal intensity. This signal enhancement is the result of the superposition of all individual optical responses of nanoplasmonic sensors. The absolute extinction intensity increased, and the peak position blue shifted ~4 nm for AuNR and ~ 0.5 nm for AuNS. Theoretically, the peak position should remain at the same position, however, the variability within plasmonic sensors contributes for this effect. Sample to sample (plasmonic sensors) variability for the LSPR position was ± 5nm for AuNR and ± 2 nm for AuNS. Although, variability from sample to sample do not compromise the sensing performance, as it is evaluated based on a peak shift variation rather than the absolute value of LSPR peak position. Optical signal amplification was achieved for multiple plasmonic sensing in series. Further evaluation of multiple sensors to achieve high signal to noise ratio (SNR) without LSPR mode coupling and peak broadening was carried out in the next studies.

Bulk sensitivity

Literature reports have demonstrated that anisotropic structures (nanorods or stars) offer higher plasmon sensitivity due to concentration of field enhancement on the tips, exhibiting higher local sensitivity when compared to isotropic (nanospheres) [22–24]. However, for large nanospheres, the increase of particle volume contributes to increase bulk sensitivity, although only by a limited extent. When the

nanostructures are deposited onto a substrate, the bulk sensitivity is also diminished because the LSPR electromagnetic field gets contained within the substrate [25].

The sensitivity to bulk RI changes was evaluated for single and multiple plasmonic sensors based on both AuNR and AuNS. Six solutions with increasing concentrations of sucrose, and different RI were injected in the system. The collected extinction spectra for the different concentrations can be seen in **Fig. 3**.

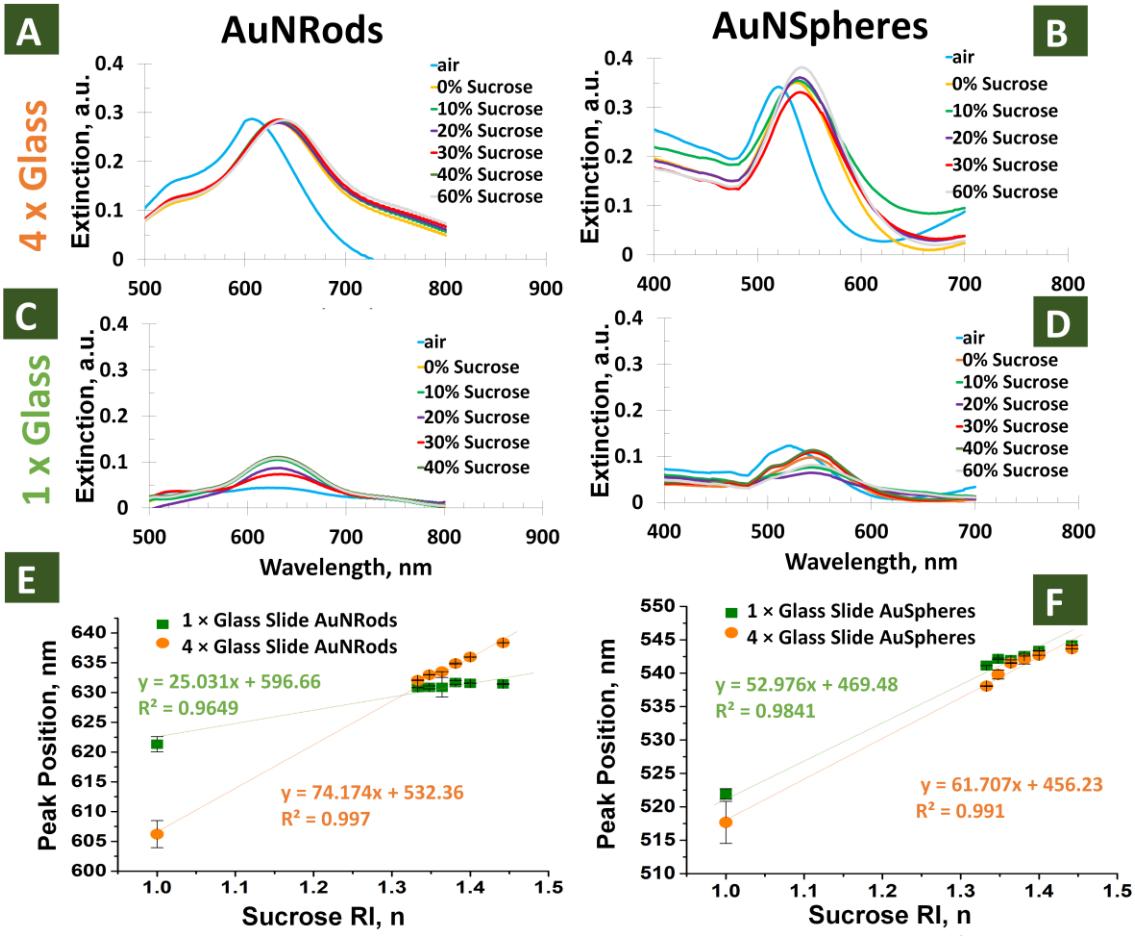

Fig. 3. Effect of single and multiple plasmonic sensors on optical response and bulk sensitivity. Spectra of 4× plasmonic sensors (A) based in AuNR and (B) based in AuNS; Spectra of 1 × plasmonic sensors (C) based in AuNR and (D) based in AuNS. Plotting of peak position *versus* RI of sucrose solutions (n=3) (E) for AuNR and (F) AuNS.

For all the conditions tested, the increase of bulk RI induced a red shift of the LSPR peak position, with AuNR based sensors showing a major shift at the longitudinal band along with small changes in the

transverse band. Single plasmonic sensors showed a sensitivity of 25.0 ± 2.7 and 52.9 ± 0.5 nm RIU^{-1} (refractive index units) for AuNR and AuNS, respectively. Whereas the alignment of 4 plasmonic sensors showed a sensitivity of 74.2 ± 5.7 and 61.7 ± 8.1 nm RIU^{-1} for AuNR and AuNS (**Fig. 3E/F**). Good reproducibility was also achieved with relative standard deviation (RSD) of 8 and 13% for AuNR and AuNS. In the case of AuNS, the sensitivity showed no significant difference between single and multiple sensors stacking. In the case of AuNR, the bulk sensitivity is 3-fold higher for multiple plasmonic sensors.

SNR can be used to calculate the accuracy of the sensors. SNR of single and multiple AuNR plasmonic sensors showed values of 5.3 and 90.43, while for AuNS similar values were obtained for single and multiple sensors (110 and 96). SNR data showed no significant improvement in terms of sensors accuracy for AuNS, in contrast for the anisotropic plasmonic sensors, higher SNR was observed for multiple plasmonic sensors. The obtained results are further discussed in the SI.

Generally, the comparison of SNR, FWHM of the LSPR peak and sensitivity data for single and multiple sensors allows to conclude that multiple sensors, unlike single plasmonic sensors, can achieve higher SNR without LSPR mode coupling and peak broadening. Even though sensing performance was improved for both type of sensors, AuNR display the best optical outcome. Therefore, multiple AuNR plasmonic sensors were selected for the following experiments.

Immobilization of DNA probe and hybridization

The immobilization of DNA probe molecules on a plasmonic transducer and further hybridization is affected by DNA length, functional linkers modified DNA and DNA probe density. DNA surface density is strongly influenced by the surface shape (flat or curved surface) as it determines the spatial arrangement of DNA on the surface. Therefore, the selected loading strategy greatly impacts the orientation and behavior of surface-immobilized DNA layers, determining the response of the nanoplasmonic sensors.

AuNR are cylindrical geometric forms with two semi-spheres at the ends. Therefore, the loading of DNA on the AuNR body and tips can behave slightly differently. For that reason, different co-immobilization strategies for probe DNA assembly followed by hybridization, were assessed.

The typical approaches to attach DNA on gold are the thiol-anchored DNA, anchoring sequences of adenine nucleotides (polyA) and/or co-immobilization with alkanethiols or organosulfur anchors of polyethylene glycol (PEG) derivatives in continuous flow [26, 27].

Prior DNA probe loading and hybridization, the nanostructures stability on the surface was assessed by monitoring the optical response over time ~1h under continuous flow of 20 µL sec^{-1} of running buffer (buffer 2). Optical signal showed a signal variation of ±0.04 nm, indicating no detectable loss of AuNR.

DNA probe immobilization strategy with thiol-modified DNA with ten adenines sequence (SH-PolyA-DNA probe), working as horizontal spacer to maintain DNA upright conformation was tested. The kinetic of SH-PolyA-DNA probe immobilization was continuously monitored by tracking the plasmon peak shift for ~10 hours (**Fig. S8** of SI). The obtained results, described in the SI, showed that 65% of probe immobilization was achieved within 1h, time selected for further experiments. However, the hybridization of fully complementary target was not favorable, with LSPR peak remaining unchanged. The unsuccessful hybridization of DNA might be related to low probe surface density due to special arrangement of DNA with poly A horizontal spacers. Hence, the low hybridization rate induces insignificant RI change. [28]

Alternatively, nanoparticles surface modification was performed with the same DNA sequence probe without the poly A spacer and co-immobilized with methoxy PEG (mPEG) of Mw 350, 800 and 2000 Da, as shown in **Fig. S9**. Two different target incubation times were also assessed. The hybridization assays providing the highest plasmon peak shift were achieved for AuNR co-immobilized with SH-DNA probe and PEG2000, as deeply explained in the SI.

Complementary fluorescence assays were also carried out to determine the surface coverage of DNA probe on the AuNR plasmonic sensors. Plasmonic sensors were exposed to SH-DNA probe/PEG of different Mw for 1h, as described in SI. The comparison of DNA concentrations between the solutions

where plasmonic sensors were incubated and the controls, allowed to estimate the surface coverage of DNA. PEG2000 showed the highest probe DNA surface coverage, $1.63 \pm 0.14 \times 10^{12}$, whereas PEG350 and 800 exhibited similar DNA loading behavior, $5.35 \pm 1.63 \times 10^{11}$ and $1.58 \pm 0.74 \times 10^{11}$, respectively. PEG2000 is shorter than the SH-DNA probe (~7 nm), being able to maintain the distance between DNA strands, minimizing electrostatic repulsion, and allowing target DNA accessibility. The decrease of the Mw of PEGs molecules, increases the exposure of the single probe DNA, and its upstand orientation starts to be affected.

AuNR co-immobilized with SH-DNA probe and PEG2000 showed the highest probe surface coverage of ~ 1.6×10^{12}, which also correspondents to the highest plasmon peak shift for hybridization. These data are consistent with the typical behavior of 15-30 oligonucleotides immobilization on flat surfaces with good hybridization efficiencies[27, 29]. Two factors contribute to this effect, the higher proportion of cylindric geometry of AuNR combined with its immobilization on a substrate. Therefore, this immobilization strategy for AuNR allowed the optimal distance between DNA strands and steric hindrance which improved the efficiency for target DNA hybridization.

DNA hybridization occurs when complementary DNA target is captured by probe DNA forming a double helix structure. The best co-immobilization strategy was then employed for this study. Similarly, to the previous tests, extinction spectra were collected in buffer before/after probe DNA loading and each standard concentration of DNA target (1h each). The optical spectra of multiple (4×) plasmonic sensors showed a longitudinal extinction peak with maximum at ~646.46 ± 0.04 nm in buffer 1, which upon co-immobilization with SH-DNA/PEG2000 red shifted 6.38 ± 0.06 nm (buffer 1), as can be seen in **Fig. 4A**. Prior hybridization, plasmonic nanosensors were exposed to the same buffer as the one used in standard DNA preparation (buffer 2). The observed blue shift of -0.11 ± 0.06 nm, is related to slightly variation of RI within immobilization and hybridization buffers.

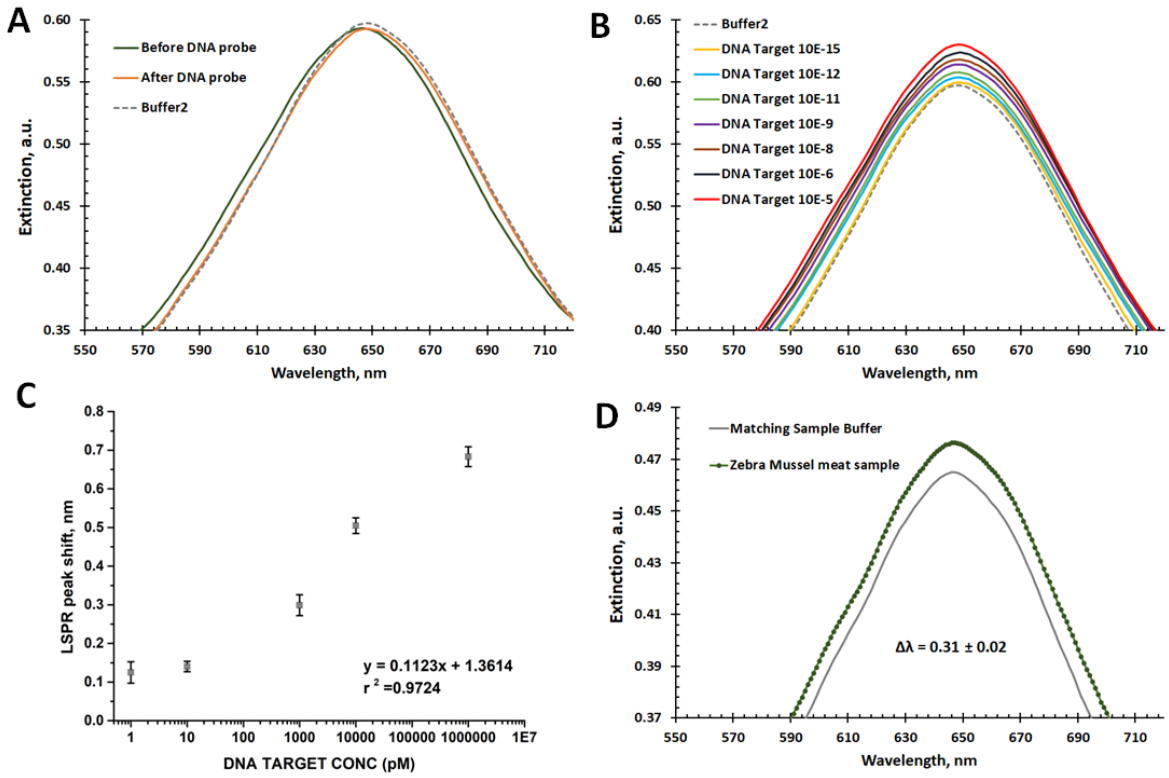

Fig. 4. LSPR spectra upon surfaces modifications. A) SH-DNA probe/PEG 2000 immobilization; B) Increasing concentrations of target DNA hybridization; C) calibration curve of peak shift *versus* DNA target concentration (peak position prior hybridization of 648.54±0.06 nm); D) Spectra in buffer 2 upon exposure of DNA extracted from Zebra Mussels meat using the NucleoSpin Food kit.

Real-time hybridization studies were carried out by sequential injection of target DNA with concentrations ranging from 1pM to 1×10^6 pM, which induced a red shift with linear behavior. The extinction spectra for the different target concentrations are displayed in **Fig. 4B**. Peak shifts to higher wavelength were observed with the lowest and highest target concentration corresponding to the yellow and red curves. Hybridization was achieved for 45 min at intermittent flow (expose to continuous flow for 10 sec and static flow for 5 min, for 7 cycles) followed by 30 min rinsing to remove target non-specific binding (**Table S2** of SI). **Fig. 4C**, displays the LSPR plasmon shifts with increasing concentrations of complementary target DNA. The hybridization profile suggests a slow binding for the first concentrations, although it consistently red shifts with the increment of target DNA molecules. Data showed a linear response of log target DNA concentration versus LSPR shift. The relation of plasmon shift with log of target DNA concentration is a typical behavior already reported for other

LSPR sensors[30, 31]. Limit of detection (LoD) based on 3 times the standard deviation of buffer 2 extinction signal (0.035) and regression equation was calculated. The microfluidic system with multiple (4×) AuNR plasmonic nanosensors showed for a short incubation time of ~45 min a LoD of 2.06 pM. As can be seen in **Table 2**, bottom-up nanosensors for ultrasensitive detection of RNA have already been reported, although these studies use long target incubation times (12h or overnight), which is not compatible with point of care or on the field analysis[32, 33]. Generally, state-of-the-art data report higher peak shifts upon target DNA binding and slightly lower detection limits than the data reported herein with our multiple sensors. However, these methods are usually based on complex and expensive fabrication techniques, require additional equipment for temperature control, or rely on enzymes, labels, or complex design of secondary DNA structures amplification[30, 34–36].

Moreover, the integration of the device in a microfluidic system offers the advantage for plasmon peak shift continuous monitoring, and by keeping the sensors exactly in the same position the analyzed regions are unaltered, eliminating errors associated with sample moving of batch systems. Another advantage is that our approach can be applied to plasmonic sensors regardless of fabrication strategy or amplification methodology, improving the existing DNA based biosensors.

374

375 **Table 2.** Literature survey on nanomaterial-based optical methods for the determination of DNA

Work	Plasmonic structure	Sensitivities nm/RIU	LoDs	Peak shift, nm Probe/target	Extra Information	Hybridization time	Capture probe	Fabrication method	Incubation
Roether[34]	mushroom-like nanostructures with silicon dioxide stems and gold caps	54	-	6.6nm/-	DNA polymerase activity	- 16h probe room temperature	SH-DNA: hexanedithiol	Au depostion, de-werring and glass etching	Using microfluidics
Masterson[37]	AuTriangular nanoprisms AuNRods AuNSpheres	318 225 135	98aM - -	35 nm/12 nm - -	RNA detection	Overnight room temperature -	SH-DNA: SH-PEG4	colloid synthesis + surface functionalization (MPTMS) on glass	Drop casting
Joshi[33]	Au nanoprisms	-	23-35 fM miR-21 100nM -50fM miR-10b	20.5nm/18.8 nm	RNA detection	12h room temperature	SH-DNA: SH-PEG6	colloid synthesis + surface functionalization (MPTMS) on glass	Drop casting
Zhu[35]	Au nano squares	100	70fM	-/82nm	DNA detection	1h (37ºC)	SH-DNA	nanoimprint technology	Using microfluidics
Nguyen[38]	Au NSpheres	~80	50fM	7.8nm /5.9 nm	DNA detection	32 min 62ºC	SH-PNA probe	colloid synthesis + surface functionalization (MPTMS) on glass	Using microfluidics
Miti[36]	Au NSpheres	-	1nM (prior amplification) 1pM after amplification	-/0.4nm/0.5 nm*	HCR Signal amplification	1h	SH-DNA probe	colloid synthesis + surface functionalization (APTES) on glass	Drop casting
Bonyar[30]	Au nanomushrooms	93 nm	5nM	9.4 nm/6.6 nm	DNA detection	2h room temperature (22ºC)	SH-DNA	Deposition of Au in pre-treated Aluminium +annealing+transfer to epoxy substrate	Drop casting
This work	AuNRods	74	2pM	2 nm/0.7nm	DNA detection	~45 min (22ºC)	SH-DNA	colloid synthesis + surface functionalization (MPTMS) on glass	Using microfluidics

*** LSPR Shift upon amplification**

376

377

The early detection though environmental DNA detection of invasive species in river basins helps to mitigate and control its spread. Our plasmonic sensor array system can be easily adapted to a portable system by using a simple transmissive optical setup device. As a proof of concept, zebra mussel samples collected from the Iznajar reservoir, in Spain, were used, assessing the system potential to detect a specific DNA sequence from these invasive species. Zebra mussel meat was extracted from the shell and used for DNA extraction. The extract was characterized and then diluted in the buffer used for hybridization step (details in experimental section of SI). Prior sample injection, the buffer used while collecting extinction spectra match the buffer concentration of the sample. Samples induced an average red shift of 0.31 ± 0.02 nm (**Fig. 4D)**, within the linear range, corresponding to a DNA target concentration of 5.1± 1.6 nM. The same sample was also analyzed by nanodrop showing a total DNA concentration of 1058 ± 20 ng/µL compared to the 0.034 ng/µL obtained with our device. Nanodrop determines the total dsDNA concentration and cannot distinguish sequences of interest within all others. As expected, these data indicates that our system detects much smaller amount of DNA molecules, which would correspond to the specific DNA sequence targeted, while the nanodrop quantifies total DNA on the extract.

Overall, our system could be extremely useful for real time monitoring of small oligonucleotides from invasive species allowing to alert authorities upon detection. Still, thoroughly experiments with real samples would still be required.

CONCLUSIONS

We demonstrated the efficacy of multiple plasmonic sensors assembled in a flow cell to significantly improve the sensitivity and accurately detect tiny peak shifts induced by short DNA sequences. This signal amplification strategy increases the overall density of nanoparticles on the surface analyzed, without introducing coupling effects, overcoming some limitations of bottom-up approaches. The combination of fours sensors resulted in higher SNR and improved sensitivity unlike single sensors, and AuNR performing better than AuNS.

Regarding hybridizations studies, sensors co-immobilized with SH-DNA probe and PEG2000 showed the highest probe surface coverage of ~ 1.6×10^{12} and the highest plasmon peak shift in the presence of target. This condition was then used to detect DNA from Zebra Mussels, reaching a detection limit of ~2.0 pM. Real samples from Zebra Mussels meat were successfully analyzed, within less than 45 min. The developed amplification approach is a simple and low-cost alternative to improve the sensing capacity of bottom-up plasmonic sensors, and it can be applied to all plasmonic sensors regardless the fabrication process.

DECLARATIONS

Funding/ Acknowledgments

This work was supported by project Nanotechnology Based Functional Solutions (NORTE-01-0145-FEDER-000019), supported by Norte Portugal Regional Operational Programme (NORTE2020), under the PORTUGAL 2020 Partnership Agreement, through the European Regional Development Fund, and by the Partnership Agreement with Confederación Hidrográfica del Guadalquivir (Spain) for the development of a system of early detection of the zebra mussel through analysis of environmental DNA.

Conflicts of interest/ Competing interests

The authors declare that they have no known competing financial interests or personal relationships that could have appeared to influence the work reported in this paper.

Authors' Contributions

Experiments were conducted by JR Guerreiro, A. Toldrà. Flow cell design, fabrication as well as microfluidic assembly and software development was conducted by A. Ipatov. Zebra Mussels specific DNA sequence identification and extraction/preparation of real samples by J. Carvalho. Conceptualization and method development were designed by J.R. Guerreiro and Marta Prado. Writing-Original draft preparation: JR Guerreiro. M. Prado participated on project administration and funding acquisition. Writing- Reviewing and Editing by JR Guerreiro, A. Ipatov, J. Carvalho, A. Toldrà, and M. Prado.

REFERENCES

1. Willets KA, Van Duyne RP (2007) Localized surface plasmon resonance spectroscopy and sensing. Annu Rev Phys Chem 58:267–297. https://doi.org/10.1146/annurev.physchem.58.032806.104607

2. Guo L, Jackman JA, Yang HH, et al (2015) Strategies for enhancing the sensitivity of plasmonic nanosensors. Nano Today 10:213–239. https://doi.org/10.1016/j.nantod.2015.02.007

3. Murray WA, Barnes WL (2007) Plasmonic materials. Adv Mater 19:3771–3782. https://doi.org/10.1002/adma.200700678

4. Scuderi M, Esposito M, Todisco F, et al (2016) Nanoscale Study of the Tarnishing Process in Electron Beam Lithography-Fabricated Silver Nanoparticles for Plasmonic Applications. J Phys Chem C 120:24314–24323. https://doi.org/10.1021/acs.jpcc.6b03963

5. Haynes CL, Van Duyne RP (2001) Nanosphere lithography: A versatile nanofabrication tool for studies of size-dependent nanoparticle optics. J Phys Chem B 105:5599–5611. https://doi.org/10.1021/jp010657m

6. Hanarp P, Kall M, Sutherland DS (2003) Optical properties of short range ordered arrays of nanometer gold disks prepared by colloidal lithography. J Phys Chem B 107:5768–5772. https://doi.org/10.1021/jp027562k

7. Rahim FA, Dong-Hwan K (2016) Nanoparticle polymer composites on solid substrates for plasmonic sensing applications. Nano Today 11:415–434. https://doi.org/10.1016/j.nantod.2016.07.001

8. Barsan MM, Brett CMA (2016) Recent advances in layer-by-layer strategies for biosensors incorporating metal nanoparticles. Trac-Trends Anal Chem 79:286–296. https://doi.org/10.1016/j.trac.2015.11.019

9. Grzelczak M, Pérez-Juste J, Mulvaney P, Liz-Marzán LM (2008) Shape control in gold nanoparticle synthesis. Chem Soc Rev 37:1783–1791. https://doi.org/10.1039/b711490g

10. Scarabelli L, Sanchez-Iglesias A, Perez-Juste J, Liz-Marzan LM (2015) A “Tips and Tricks” Practical Guide to the Synthesis of Gold Nanorods. J Phys Chem Lett 6:4270–4279. https://doi.org/10.1021/acs.jpclett.5b02123

11. Navarro JRG, Lerouge F (2017) From gold nanoparticles to luminescent nano-objects: experimental aspects for better gold-chromophore interactions. Nanophotonics 6:71–92. https://doi.org/10.1515/nanoph-2015-0143

12. Guerreiro JRL, Frederiksen M, Bochenkov VE, et al (2014) Multifunctional biosensor based on localized surface plasmon resonance for monitoring small molecule-protein interaction. ACS Nano 8:7958–7967. https://doi.org/10.1021/nn501962y

13. Morsin M, Umar AA, Salleh MM, et al (2012) High Sensitivity Localized Surface Plasmon Resonance Sensor of Gold Nanoparticles : Surface Density Effect for Detection of Boric Acid. 10th IEEE Int Conf Semicond Electron 352–356. https://doi.org/10.1109/SMElec.2012.6417158

14. Tu MH, Sun T, Grattan KT V (2012) Optimization of gold-nanoparticle-based optical fibre surface plasmon resonance (SPR)-based sensors. Sensors and Actuators B-Chemical 164:43–53. https://doi.org/10.1016/j.snb.2012.01.060

15. Lowe S, Browne M, Boudjelas S, De Poorter M (2000) 100 of the World's Worst Invasive Alien Species A selection from the Global Invasive Species Database. Invasive Species Spec Gr

16. Carvalho J, Garrido-Maestu A, Azinheiro S, et al (2021) Faster monitoring of the invasive alien species (IAS) Dreissena polymorpha in river basins through isothermal amplification. Sci Rep 11:10175. https://doi.org/10.1038/s41598-021-89574-w

17. EU (2014) Regulation (EU) No 1143/2014 of the European Parliament and of the Council of 22 October 2014 on the prevention and management of the introduction and spread of invasive alien species. 35–55

18. Wang YY, Tang L (2013) Chemisorption assembly of Au nanorods on mercaptosilanized glass substrate for label-free nanoplasmon biochip. Anal Chim Acta 796:122–129. https://doi.org/10.1016/j.aca.2013.08.024

19. Chen HJ, Shao L, Li Q, Wang JF (2013) Gold nanorods and their plasmonic properties. Chem Soc Rev 42:2679–2724. https://doi.org/10.1039/c2cs35367a

20. Malinsky DM, Kelly KL, Schatz GC, Van Duyne RP (2001) Nanosphere Lithography: Effect of Substrate on the Localized Surface Plasmon Resonance Spectrum of Silver Nanoparticles. J Phys Chem B 105:2343–2350. https://doi.org/10.1021/jp002906x

481 21. Ray PC, Fan Z, Crouch RA, et al (2014) Nanoscopic optical rulers beyond the FRET distance limit:
482 fundamentals and applications. Chem Soc Rev 43:6370–6404. https://doi.org/10.1039/C3CS60476D

483 22. Chen H, Kou X, Yang Z, et al (2008) Shape- and size-dependent refractive index sensitivity of gold
484 nanoparticles. Langmuir 24:5233–5237. https://doi.org/10.1021/la800305j

485 23. Nehl CL, Liao HW, Hafner JH (2006) Optical properties of star-shaped gold nanoparticles. Nano Lett
486 6:683–688. https://doi.org/10.1021/nl052409y

487 24. Lee KS, El-Sayed MA (2006) Gold and silver nanoparticles in sensing and imaging: Sensitivity of
488 plasmon response to size, shape, and metal composition. J Phys Chem B 110:19220–19225.
489 https://doi.org/10.1021/jp062536y

490 25. Murray WA, Auguie B, Barnes WL (2009) Sensitivity of Localized Surface Plasmon Resonances to
491 Bulk and Local Changes in the Optical Environment. J Phys Chem C 113:5120–5125.
492 https://doi.org/10.1021/jp810322q

493 26. Steel AB, Levicky RL, Herne TM, Tarlov MJ (2000) Immobilization of Nucleic Acids at Solid
494 Surfaces : Effect of Oligonucleotide Length on Layer Assembly. Biophys J 79:975–981.
495 https://doi.org/10.1016/S0006-3495(00)76351-X

496 27. Sohreiner SM, Shudy DF, Hatoh AL, et al (2010) Controlled and efficient hybridization achieved with
497 DNA probes immobilized solely through preferential DNA-substrate interactions. Anal Chem 82:2803–
498 2810. https://doi.org/10.1021/ac902765g

499 28. Lu W, Wang L, Li J, et al (2015) Quantitative investigation of the poly-adenine DNA dissociation from
500 the surface of gold nanoparticles. Sci Rep 5:1–9. https://doi.org/10.1038/srep10158

501 29. Herne TM, Tarlov MJ (1997) Characterization of DNA probes immobilized on gold surfaces. J Am
502 Chem Soc 119:8916–8920. https://doi.org/10.1021/ja9719586

503 30. Bonya A (2020) Large Scale Fabrication of Ordered Gold Nanoparticle − Epoxy Surface
504 Nanocomposites and Their Application as Label-Free Plasmonic DNA Biosensors. ACS Appl Mater
505 Interfaces 12:4804–4814. https://doi.org/10.1021/acsami.9b20907

506 31. Guerreiro JRL, Teixeira N, De Freitas V, et al (2017) A saliva molecular imprinted localized surface
507 plasmon resonance biosensor for wine astringency estimation. Food Chem 233:457–466.

https://doi.org/10.1016/j.foodchem.2017.04.051

32. Masterson AN, Liyanage T, Kaimakliotis H, et al (2020) Bottom-Up Fabrication of Plasmonic Nanoantenna-Based High-throughput Multiplexing Biosensors for Ultrasensitive Detection of microRNAs Directly from Cancer Patients' Plasma. Anal Chem 92:9295–9304. https://doi.org/10.1021/acs.analchem.0c01639

33. Joshi GK, Deitz-Mcelyea S, Johnson M, et al (2014) Highly specific plasmonic biosensors for ultrasensitive MicroRNA detection in plasma from pancreatic cancer patients. Nano Lett 14:6955–6963. https://doi.org/10.1021/nl503220s

34. Roether J, Chu KY, Willenbacher N, et al (2019) Real-time monitoring of DNA immobilization and detection of DNA polymerase activity by a microfluidic nanoplasmonic platform. Biosens Bioelectron 142:111528. https://doi.org/10.1016/j.bios.2019.111528

35. Zhu S, Li H, Yang M, Pang SW (2018) Label-free detection of live cancer cells and DNA hybridization using 3D multilayered plasmonic biosensor. Nanotechnology 29:365503. https://doi.org/10.1088/1361-6528/aac8fb

36. Miti A, Thamm S, Müller P, et al (2020) A miRNA biosensor based on localized surface plasmon resonance enhanced by surface-bound hybridization chain reaction. Biosens Bioelectron 167:112465. https://doi.org/https://doi.org/10.1016/j.bios.2020.112465

37. Masterson AN, Liyanage T, Kaimakliotis H, et al (2020) Bottom-Up Fabrication of Plasmonic Nanoantenna-Based High-throughput Multiplexing Biosensors for Ultrasensitive Detection of microRNAs Directly from Cancer Patients' Plasma. Anal Chem 92:9295–9304. https://doi.org/10.1021/acs.analchem.0c01639

38. Nguyen AH, Sim SJ (2015) Nanoplasmonic biosensor: detection and amplification of dual bio-signatures of circulating tumor DNA. Biosens & Bioelectron 67:443–449. https://doi.org/10.1016/j.bios.2014.09.003